

On turbulent particle fountains

Nicola Mingotti and Andrew W. Woods †,

BP Institute, University of Cambridge, Madingley Road, Cambridge CB3 0EZ, UK

(Received ?; revised ?; accepted ?. - To be entered by editorial office)

We describe new experiments in which particle-laden turbulent fountains with source Froude numbers $20 > Fr_0 > 6$ are produced when particle-laden fresh water is injected upwards into a reservoir filled with fresh water. We find that the ratio U of the particle fall speed to the characteristic speed of the fountain determines whether the flow is analogous to a single-phase fountain ($U \ll 1$) or becomes a fully separated flow ($U \geq 1$). In the single-phase limit, a fountain with momentum flux M and buoyancy flux B oscillates about the mean height, $h_m = (1.56 \pm 0.04)M^{3/4}B^{-1/2}$, as fluid periodically cascades from the maximum height, $h_t = h_m + \Delta h$, to the base of the tank. Experimental measurements of the speed u and radius r of the fountain at the mean height h_m , combined with the conservation of buoyancy, suggest that $Fr(h_m) = u(g'r)^{-1/2} \approx 1$. Using these values, we find that the classical scaling for the frequency of the oscillations, $\omega \sim BM^{-1}$ is equivalent to the scaling $u(h_m)/r(h_m)$ for a fountain supplied at $z = h_m$ with $Fr = 1$ (Burridge & Hunt 2013). This suggests that the oscillations are controlled in the upper part of the fountain where $Fr \leq 1$, and that they may be understood in terms of a balance between the upward supply of a growing dense particle cloud, at the height where $Fr = 1$, and the downward flow of this cloud. In contrast, in the separated flow regime, we find that particles do not reach the height at which $Fr = 1$: instead, they are transported to the level at which the upward speed of the fountain fluid equals their fall speed. The particles then continuously sediment while the particle-free fountain fluid continues to rise slowly above the height of particle fallout, carried by its momentum.

Key words: Particles, fountains, suspensions

1. Introduction

The dynamics of high Reynolds number turbulent fountains have been the focus of considerable attention owing to their relevance to a variety of natural and industrial processes, including supply of air-flows from underfloor cooling systems (Lin & Linden 2005; Liu & Linden 2006), refuelling of vessels (Carazzo *et al.* 2010), and replenishment of magma chambers (Campbell & Turner 1989). Following the pioneering work of Turner (1966), numerous studies have proposed scaling laws and models for the height of rise and the speed in the fountain and these have been tested experimentally (Hunt & Burridge 2015). Fountains are often characterised in terms of the Froude number at the source, $Fr_0 = u_0/(g'_0 r_0)^{1/2}$, where r_0 and u_0 are the source radius and velocity and $g'_0 = g\Delta\rho_0/\rho$ is the buoyancy of the fluid at the source. With $Fr_0 > 4$, fountains are able to entrain a significant mass of ambient fluid, and the height of rise, speed and frequency of oscillation depend primarily on the source momentum flux, $M = u_0^2 r_0^2$, and source buoyancy flux,

† Email address for correspondence: andy@bpi.cam.ac.uk

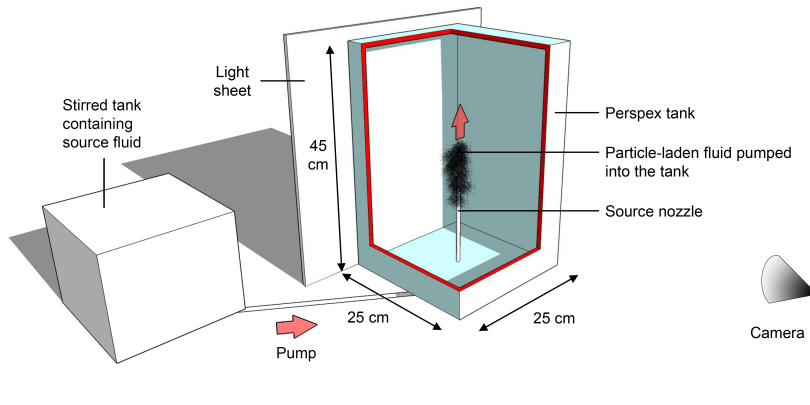


FIGURE 1. Schematic of the experimental setup.

$B = g'_0 u_0 r_0^2$. In contrast, with small source Froude number, $Fr_0 < 1$, there is much less entrainment, and the properties of the fountain depend primarily on the source velocity, u_0 , radius, r_0 and buoyancy g'_0 . The rise height of turbulent fountains is characterised by periodic oscillations of a frequency ω . Detailed measurements suggest that in the case $Fr_0 < 1$, $\omega = f(Fr) u_0 / r_0$, whereas in the case $Fr_0 > 4$, $\omega \sim B/M$ (Burrige & Hunt 2013).

In explosive volcanic eruptions, two-phase fountains develop when a dense mixture of particles and gas issues from the volcano (Woods 2010). Although theoretical models have been developed to describe the dynamics of such volcanic fountains, these models are often based on the assumption of single-phase flow, and in many cases they focus on the potential reversal of buoyancy as air is entrained and heated by the ash. One exception is the recent experimental study by Carazzo *et al.* (2015), who carried out a series of experiments in which particle-laden hot air was supplied to the base of a room containing cooler air. They explored the partitioning of the particles as some fell from the flow, while the remaining mixture of the particles and hot air became buoyant. The experimental results were compared with the predictions of a numerical model of a rising fountain with reversing buoyancy. However, there is more to learn about the dynamics of particle-laden fountains, which, as well as being related to volcanic eruptions, are of fundamental interest for industrial fluidisation-type processes in which jets of fluid are used to suspend particles.

The purpose of this work is to present a series of experiments in which a jet of fresh water laden with heavy particles is supplied to the base of a tank containing fresh water, and to compare the dynamics of such a particle-laden fountain with those of an equivalent salt fountain. We show that the ratio U of the particle fall speed to the characteristic fountain speed distinguishes between conditions in which the particle-laden flow behaves effectively as a single-phase fluid, $U \ll 1$, and conditions in which the two phases separate owing to particle fallout, $U > 1$. Also, using new measurements, we recognise that at the mean height of a single-phase fountain, $Fr \approx 1$ and so the amplitude of the oscillations of the height of the fountain, Δh , is similar to the fountain radius at the mean height of the fountain. In the limit $U \ll 1$, this leads to a picture of fountain oscillations being controlled by the periodic accumulation and collapse of fluid at the fountain top, where $Fr < 1$. In contrast, in the limit $U > 1$, the particles separate from the fountain fluid while $Fr > 1$ and since the fluid still has a significant upward momentum, it continues upwards.

Exp.	$M \times 10^{-7}$	$B \times 10^{-7}$	$A \times 10^{-5}$	Re	Fr_0	$St \times 10^{-4}$	D	$v_s \times 10^{-3}$	U
1	5.57	1.01	5.41	462	8.99	0.05	18	0.40	0.034
2	5.57	0.68	5.41	462	11.01	0.03	18	0.40	0.042
3	8.01	0.81	5.41	554	13.22	0.03	18	0.40	0.042
4	2.00	0.41	5.41	277	6.60	0.06	18	0.40	0.042
5	3.57	0.54	5.41	370	8.81	0.04	18	0.40	0.042
6	5.57	0.34	5.41	462	15.58	0.02	18	0.40	0.059
7	3.57	0.27	5.41	370	12.46	0.02	18	0.40	0.059
8	8.11	2.70	2.38	558	11.02	0.44	40	1.89	0.109
9	8.11	1.35	2.38	558	15.59	0.22	40	1.89	0.154
10	8.11	1.62	2.38	558	14.23	0.42	50	3.02	0.225
11	8.01	1.22	5.41	554	10.79	0.32	50	3.02	0.259
12	8.11	0.81	2.38	558	20.12	0.21	50	3.02	0.318
13	8.11	1.89	2.38	558	13.18	1.11	75	6.80	0.469
14	8.01	1.83	5.41	554	8.81	1.09	75	6.80	0.476
15	8.11	1.38	2.38	558	15.44	0.81	75	6.80	0.549
16	8.11	1.08	2.38	558	17.43	0.64	75	6.80	0.621
17	8.01	0.93	5.41	554	12.32	0.55	75	6.80	0.667
18	8.11	0.81	2.38	558	20.12	0.48	75	6.80	0.717
19	8.11	2.43	2.38	558	11.61	2.86	106	13.58	0.827
20	8.01	0.60	5.41	554	15.41	0.36	75	6.80	0.831
21	8.11	1.89	2.38	558	13.18	2.22	106	13.58	0.937
22	8.01	1.83	5.41	554	8.81	2.18	106	13.58	0.950
23	8.01	1.50	5.41	554	9.72	1.79	106	13.58	1.049
24	8.11	1.49	2.38	558	14.86	1.75	106	13.58	1.056
25	8.01	1.24	5.41	554	10.68	1.48	106	13.58	1.154
26	8.11	1.24	2.38	558	16.25	1.46	106	13.58	1.157
27	8.01	0.96	5.41	554	12.14	1.14	106	13.58	1.311
28	8.11	0.95	2.38	558	18.63	1.12	106	13.58	1.322
29	8.01	0.81	5.41	554	13.22	0.96	106	13.58	1.428
30	8.11	0.78	2.38	558	20.46	0.92	106	13.58	1.459

TABLE 1. Conditions of the particle fountain experiments. We let M (m^4/s^2) denote the momentum flux at the source, while B (m^4/s^3) is the downward buoyancy flux at the source, A (m^2) is the cross-sectional area of the nozzle, D (μm) and v_s (m/s) are the diameter and settling speed of the particles and $U = v_s M^{\frac{1}{4}} B^{-\frac{1}{2}}$ is the ratio between the particle fall speed and the characteristic fountain speed given by equation 2.1. Re , Fr_0 and St are the Reynolds, Froude and Stokes numbers associated with the particle-laden flow at the source (Williamson *et al.* 2008; Hunt & Burrige 2015).

2. Experiments

We carried out a series of experiments in a tank of dimension $25 \times 25 \times 45$ cm (figure 1). The tank was filled with fresh water, and a source nozzle was placed in the centre of its base. To observe the impacts of different source conditions, two round nozzles of diameter 5.5 and 8.3 mm were used in the experiments (see table 1). During each experiment, one of the nozzles was connected to a stirred tank containing a suspension of water and silicon carbide particles (Washington Mills). The suspension of particles used in each experiment was monodisperse; however, particles of different sizes were used in different experiments to observe the impacts of different particle fall speeds. Table 1 shows that the diameter D of the particles used in the experiments ranged between 18 and 106 μm . Five settling experiments were run to measure the fall speeds of these particles in water, using the method described in Mingotti & Woods (2015). These experiments indicated that particles of different diameters settled at different speeds, ranging between 0.4 and

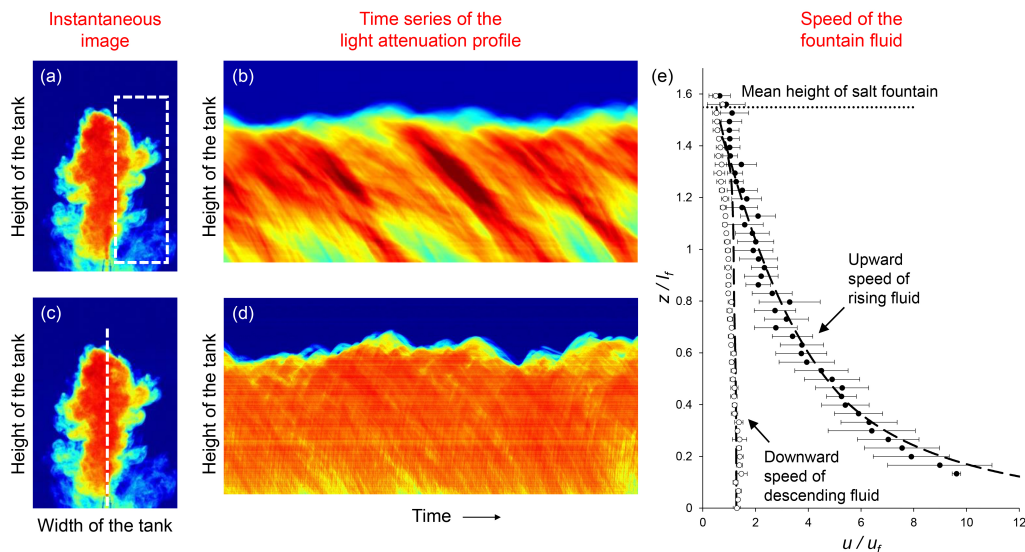


FIGURE 2. (a) False colour image of a photograph of a typical fountain. For each photograph captured during an experiment, we measured the instantaneous profile of light attenuation along the fountain centerline, as well as the horizontally-averaged profile in the region near the flanks of the fountain (shown by the dashed white lines in figures c and a respectively). We then plotted the time series of these profiles (figures d and b respectively). The inclined lines across which the light intensity changes in these figures illustrate the upward and downward motion of parcels of dyed fluid in the tank. We used the Hough transform to measure the gradient of the upward- and downward-sloping lines in these images, and thereby estimate the time-averaged velocities of the rising and descending fluid. In figure e, solid and open circles are used to plot the average velocities which were measured during our experiments (table 1), scaled by the characteristic fountain speed u_f (equation 2.1).

13.6 mm/s (table 1), in good agreement with the range of expected Stokes terminal velocities. In all experiments, the fall speed of the particles was much smaller than the speed of the fountain fluid at the source (see table 1, $St \ll 1$). Consequently, particles rapidly acquired the flow speed and behave like tracers in the fluid in the region above the source.

The particle-laden fluid was supplied to the experimental tank using a peristaltic pump (Watson Marlow) at a number of different flow rates, ranging between 4 and 8 cm³/s. In our experiments, the outflow from the nozzle rapidly became turbulent; however, in the pipe feeding the nozzle, the flow might not be fully turbulent and this might have an impact on the source momentum flux (Baines *et al.* 1990). Following Baines *et al.*, whose experiments had similar source conditions to the present study, we assumed the flow through the nozzle to be laminar, and estimated the source momentum flux by calculating the equivalent momentum of a flow with constant velocity across a hole with diameter 0.83 times the nozzle diameter. However, in all figures, error bars are shown to include the possibility that the flow in the nozzle is in fact turbulent. We also note that in the majority of our experiments, the Froude number at the source was in the range $Fr_0 \approx 6 - 20$ and the Reynolds number, $Re \approx 460 - 560$ (table 1). This is consistent with the motion of the fountain fluid becoming turbulent on leaving the source and the motion being controlled by the momentum and buoyancy fluxes, M and B (Williamson *et al.* 2008).

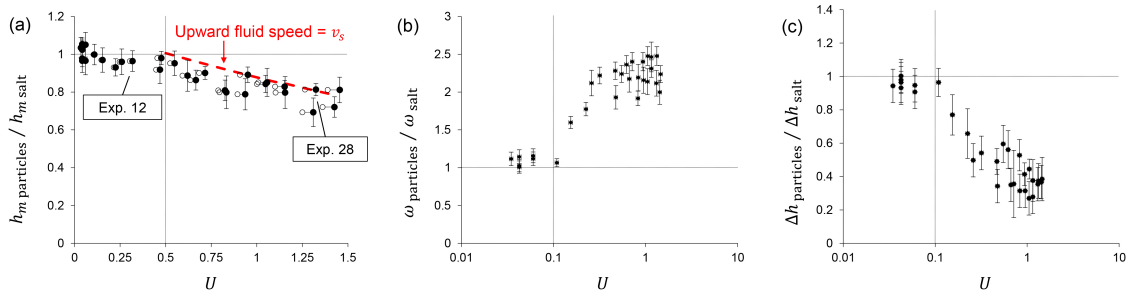


FIGURE 3. (a) Height of rise, (b) frequency and (c) amplitude of the oscillations in particle-laden fountains relative to those in salt fountains, for a range of different particle settling speeds relative to the fountain speed. In figure a, closed circles are used to illustrate the ratio between the particle fall speed and the fountain speed assuming the flow in the nozzle is laminar, while, for comparison open circles illustrate the same ratio if we assume that the flow in the nozzle is turbulent (Baines *et al.* 1990). In figures b and c, we assume the flow is laminar in the nozzle, but include horizontal error bars to illustrate the uncertainty associated with the source condition.

The tank was backlit using a light sheet (LightTape by Electro-LuminX Lighting Corp.). During an experiment, the light emitted by the sheet was attenuated across the tank containing particle-laden fluid. We typically used particle concentrations of order 1-10 g/litre at the source: within this range of concentrations, light attenuation could be detected using a Spark SP-5000M-USB camera located on the opposite side of the tank (figure 1). To observe the motion of the fountain fluid over time, we captured images at a frequency 200 Hz. For calibration purposes and to test our experimental results with the existing models (including those given by Mizushima *et al.* 1982, Bloomfield & Kerr 2000 and Burrige & Hunt 2013), we repeated some of the experiments listed in table 1 using the same momentum and buoyancy fluxes, but with a saline solution as the source fluid in order to generate a single-phase fountain. Photographs captured during each experiment were analysed to measure: (i) the speed of the rising and of the descending fluid in the fountain, (ii) the time-averaged mean and maximum fountain heights, and (iii) the frequency and the amplitude of oscillations in the fountain height.

Depending on the volume flux and on the bulk density of the source fluid, the fountains in our experiments were typically 4-10 cm tall and 3-7 cm wide, and since the reservoir used for the experiments was much larger (see figure 1), we expect that there were no significant confinement effects.

2.1. Salt Fountains

Figure 2 shows how the speed of the fountain fluid was measured in an experiment. For each photograph captured during the experiment, we initially considered a portion of the image near the outer flank of the fountain (figure 2a), and measured the horizontally-averaged profile of light attenuation in this region. We show a time series of light attenuation profiles in figure 2b. In this image, parcels of saline fluid which descend from the top of the fountain towards the base of the tank lead to a descending front across which there is a change in the light intensity. Following Rocco & Woods (2015), we used the Hough transform as available in Matlab to identify these fronts, calculate their gradient and thereby estimate the speed of the descending parcels of saline fluid as a function of the vertical distance z above the source. By calculating the speed of many such fronts, we can estimate the average speed as a function of height above the source (white circles in figure 2e). We repeated the process to measure the upward speed of the saline fluid in the

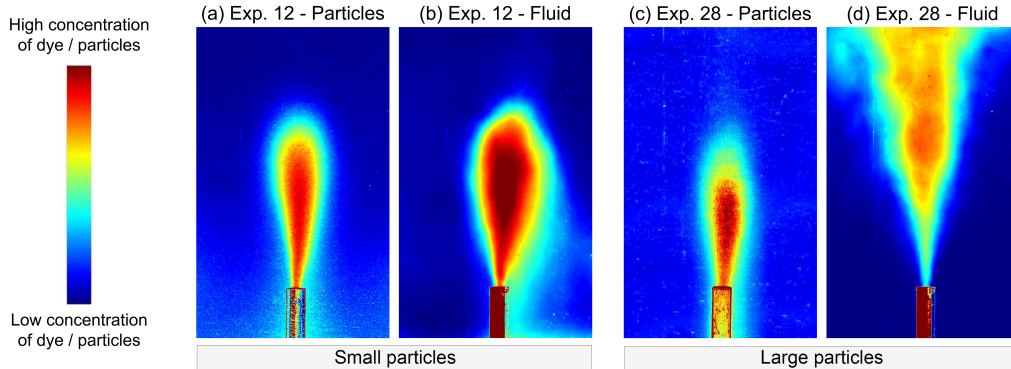


FIGURE 4. Time average of (a, c) the particles and (b, d) the dyed fluid in a particle-laden fountain, as obtained for the case (a, b) $U = 0.32$ and (c, d) $U = 1.32$. In (a, c) the fluid was undyed, so that the images reflect the particle load while in experiments (b, d) the source fluid was dyed so the images reflect the concentration of the fluid, integrated through the field of view of the fountain.

core of the fountain by plotting a time series of the light attenuation on the vertical axis of the fountain (figures 2c and d). By averaging the gradient of the forward sloping lines in this image, we estimated the mean velocity profile in the centre of the fountain (black circles in figure 2e). We note that in plotting the experimental data, we have scaled the speed with the scaling for the fountain speed based on the buoyancy and momentum flux, u_f , where

$$u_f = B^{\frac{1}{2}} M^{-\frac{1}{4}} \quad (2.1)$$

where B and M are the buoyancy and momentum flux at the source respectively (see table 1). Within experimental error, the data seem to follow a universal curve using this scaling, and this is consistent with the picture of a turbulent fountain for which $Fr \gg 1$, as proposed by Turner (1966). Figure 2e also shows that the measured velocity profiles are in good accord with data collected by Mizushima *et al.* (1982), and with the predictions of the integral model of a fountain proposed by McDougall (1981) and Bloomfield & Kerr (2000) (dashed lines). In plotting figure 2e, we scaled heights with the characteristic length scale l_f given by

$$l_f = M^{\frac{3}{4}} B^{-\frac{1}{2}} \quad (2.2)$$

Our experimental results indicate that the top height h_t and the mean height h_m of a single-phase fountain scale with l_f , with constants of proportionality $\lambda_t = 1.68 \pm 0.05$ and $\lambda_m = 1.56 \pm 0.04$ respectively, in accord with Turner (1966) and Hunt & Burridge (2015) in the range $20 > Fr > 6$. By injecting a number of pulses of dyed fluid at the source of a transparent salt fountain, we observed the rising fluid in the core of the fountain and found that at the mean height of the fountain, h_m , the inner fountain radius is $r(h_m) = (0.155 \pm 0.007) h_m$, in accord with Mizushima *et al.* (1982). Using a Fourier transform on a time series of the rise height of our salt fountains, we determined that the dominant frequency of oscillations scales as $\omega_{salt} = (0.48 \pm 0.02) u_f / l_f$ in accord with Turner (1966) and Burridge & Hunt (2013).

2.2. Particle Fountains

Having tested our experimental approach, we carried out a series of particle fountain experiments. We systematically varied the particle load and size, and the source mass

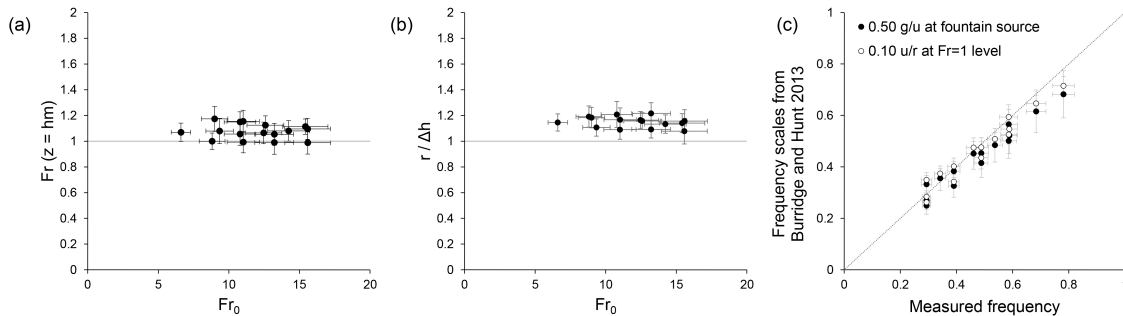


FIGURE 5. (a) Estimate of the Froude number at a height h_m above the source in our experiments; (b) Experimental measurements of the ratio between the fountain inner radius $r(h_m)$ and the amplitude of the oscillations in the fountain rise height Δh ; (c) The frequencies of the oscillations which were measured during the experiments (Hz) are compared with: (i) the expected frequencies estimated using the classic scaling for turbulent fountains based on the source conditions (black circles), and (ii) the expected frequencies estimated using the scaling for weak fountains given by Burrige & Hunt (2013) and the properties of the flow measured at the height h_m above the source (white circles).

and momentum flux so that the ratio of the fall speed of the particles relative to the characteristic fountain speed, $U = v_s/u_f$, took values in the range 0.03 to 1.5 (see table 1). In figure 3a we illustrate the variation with U of the mean height of rise of the particle fountains, h_m , as a fraction of the height of the corresponding single-phase fountains. In figures 3b and c we illustrate the frequency ω and the amplitude Δh of the oscillations at the top of the particle fountains, again shown as a fraction of the values for the equivalent salt fountains. It is seen that for $U < 0.1$, the particle fall speed is so small compared with the fountain speed, that the particle-laden fluid behaves essentially as a single-phase fluid. In this limit, the height of rise of the fountain and the amplitude of the oscillations scale with l_f , while the frequency of the oscillations scales as $B/M = u_f/l_f$.

However, our experiments indicate that for $U > 0.4 - 0.5$, the mean height of rise of a particle fountain is smaller than that of the equivalent salt fountain (figure 3a). This happens because for $U > 0.5$ the particles separate from the fountain fluid and fallout. Figure 4 illustrates the time-averaged distributions of the particles and of the fountain fluid in two experiments with different particle to fluid speed ratios ($U_1 = 0.32$ and $U_2 = 1.32$ respectively, see table 1). To make this figure, we repeated each experiment using clear and then dyed particle-laden water as the source fluid, so that the fate of the particles and the fluid could be independently tracked. Each image in the figure represents the time-averaged distribution of the particles/fluid over 30s, and uses false colours to illustrate the different concentrations of particles/dye in the tank during this time. Figures 4a and b show that for $U < 0.5$, both the small particles and the fountain fluid rose to a maximum height and then collapsed as a bulk to the floor. It is seen that the two time-averaged images overlap considerably although the fluid is somewhat more dispersed radially than the particles. In contrast, figures 4c and d show that for $U > 0.5$ the larger particles remained in a close neighbourhood of the fountain centerline as they cascaded down to the floor, while the fountain fluid continued to rise above the particle zone driven by its momentum. This is not a conventional fountain collapse, but a process of separation of the fluid and particles.

For each experiment in the separated flow regime, we used the data provided by Mizushima *et al.* (1982), which are in good agreement with the predictions of the model

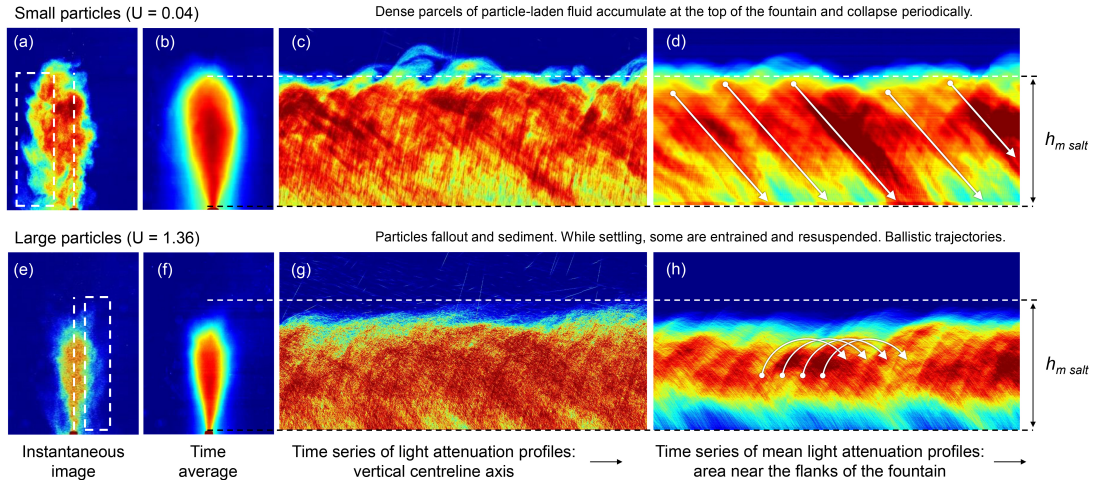


FIGURE 6. Fountains laden with particles of different sizes (experiments 3 and 29 in table 1). For each experiment, we plot: (a, e) an image which illustrates the distribution of particles in the tank at a given time during the experiment (cf. salt experiment depicted in figure 2a); (b, d) a time-averaged image showing the mean distribution of particles during 30s; (c, g) a time series of the vertical profiles of light attenuation along the centerline (cf. salt experiment depicted in figure 2d); and (d, h) a time series of the horizontally-averaged profiles of light attenuation in the region near the flanks of the fountain (cf. salt experiment depicted in figure 2b).

developed by Bloomfield & Kerr (2000), to estimate the upward speed of the fluid in the core of the fountain at different levels above the source nozzle (see figure 2e). We then identified the height at which this speed matches the fall speed of the particles, v_s , and include this theoretical curve in figure 3a as a function of U (red dashed line). It is seen that the heights of rise of the particles in the separated flow regime are similar to this model prediction, and this suggests that particles do not rise beyond the point at which their fall speed equals the ascent speed of the rising flow in the fountain.

On reaching this level, the particles continuously fallout and settle to the floor, and so the oscillations which are characteristic of the top of a single-phase fountain are suppressed. Indeed, figure 3c shows that as U increases beyond the value $U \approx 0.1$, the amplitude of the oscillations at the top of the particle fountain rapidly decreases compared to that of the corresponding salt fountains, while the frequency of the oscillations increases (figure 3b). Our experimental results suggest that there is a smooth transition between the pseudo-single-phase flow regime and the separated flow regime as U increases from 0.1 to 0.4–0.5. Over this range, the mean heights of the particle fountains decrease from $h_{m, salt}$ to $h_{m, salt} - \Delta h$ (figure 3a), where Δh is the amplitude of the oscillations of the equivalent salt fountains.

3. Discussion

In order to build insight as to why for $U > 0.5$ particle-laden fountains do not appear to exhibit the strong oscillatory behaviour seen in purely saline fountains, we have measured some further properties of the oscillations in saline fountains and fountains laden with very small particles ($U \ll 1$). In particular, we have combined (i) new measurements of the inner radius, r , and the speed, u , of the fountain at the mean height h_m , with (ii) an estimate of the buoyancy of the fountain fluid at this height using a dimensionless model for the buoyancy in a fountain based on experimental measurements as reported

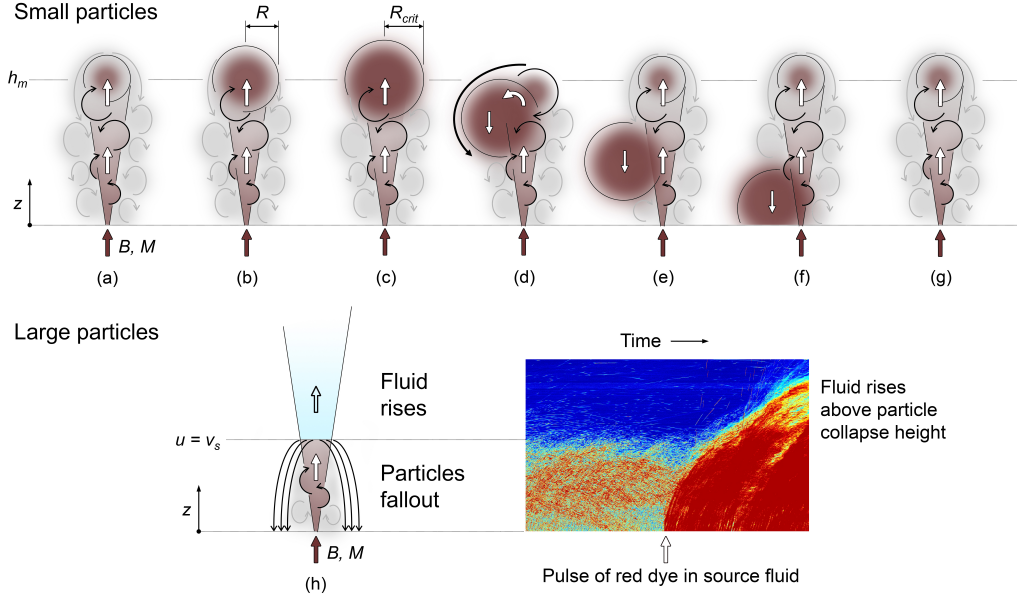


FIGURE 7. Cartoons illustrating the different mechanisms of collapse of a fountain laden with smaller or larger particles.

by Mizushima *et al.* (1982), to determine the Froude number at the mean height of rise, $Fr(h_m)$. We have found that for single-phase fountains, the local Froude number is given by

$$Fr(h_m) = \frac{u(h_m)}{[g'r(h_m)]^{1/2}} = 1.06 \pm 0.12 \quad (3.1)$$

as plotted in figure 5a.

In their experimental study, Burridge & Hunt (2013) measured the frequency of the oscillation of weak saline fountains for which the source condition was $Fr_0 = 1$, and found $\omega = (0.10 \pm 0.028) u/r$, where u and r are the speed and the radius of the fountain fluid at the source. They argued that this is distinct from the oscillations which develop in a fountain for which $Fr_0 \gg 1$. However, if we apply the Burridge-Hunt result, but using as source conditions the measured speed, buoyancy and radius of the fountain fluid at the height h_m , where we have shown that $Fr \approx 1$, then we find that the predicted frequency is in very good accord with our observations (see the open circles in figure 5c). Predictions based on the classical scaling for fountains with $Fr_0 > 5$ are also in good accord with the observations: in figure 5c we use solid circles to plot the expected frequencies of oscillation $\omega = (0.5 \pm 0.103) g'_0/u_0 \sim B/M$, in which g'_0 and u_0 are the buoyancy and the speed of the fluid at the source of the fountain (Turner 1966).

The coincidence of the experimental data and the scaling for the frequency based on the fountain properties at $Fr = 1$ suggests that oscillations in a salt fountain or in a fountain laden with small particles ($U \ll 1$) arise from a balance between the supply of new dense fluid and the convective settling of this fluid at the top of the fountain, in the region $Fr < 1$ (see figure 6d and figure 7). Fluid which is supplied by the fountain with $Fr = 1$ at $z = h_m$ will continue to rise to the maximum height h_t prior to exhausting its kinetic energy. A cloud of fountain fluid will then build up at the top of the fountain (figures 7a-c), and it will gradually begin to descend to the floor. We expect that once the

downward volume flux of this cloud exceeds the volume flux supplied from the fountain, then a discrete parcel of fluid will descend from the top of the fountain (figures 7c-f), and the cycle will repeat. If we let R denote the effective radius of one such parcel of dense fluid, modelled as a sphere, then we expect that this radius will increase over time according to

$$\frac{d}{dt} \left(\frac{4}{3} \pi R^3 \right) = Q_f \quad (3.2)$$

where

$$Q_f \sim \gamma M^{\frac{5}{4}} B^{-\frac{1}{2}} \quad (3.3)$$

is the volume flux supplied at the top of the fountain. The convective fall speed of the growing parcel of dense fluid scales as $\alpha(g'R)^{1/2}$ where α is a constant of proportionality which we estimate as $\alpha = 0.8 \pm 0.15$ from our experiments (e.g. figure 2e). When multiplied by the horizontal cross-sectional area, we estimate that the parcel has downward volume flux $\alpha\pi(g'R^5)^{1/2}$ which exceeds the supply rate from the fountain Q_f when $R > R_{crit}$ where

$$\alpha(g'R_{crit})^{\frac{1}{2}} \pi R_{crit}^2 = Q_f \quad (3.4)$$

At this stage, the volume of dense fluid may fall to the base of the tank (figures 7d-f), and a new volume will start developing (figures 7g). Using a combination of equations 3.2-3.4, we calculate that the period t between two oscillations in the fountain rise height is given by

$$t = \frac{1}{\omega} = \frac{4}{3} \frac{\gamma^{4/5}}{\pi^{1/5} \alpha^{6/5}} \frac{M}{B} \quad (3.5)$$

and using the speed and frequency data which we measured in our experiments (figures 3a and b respectively), we estimate that $\gamma = 1.73 \pm 0.26$.

In the case of separated flow, $U > 0.5$, the particle fall speed is sufficiently large that at the maximum height reached by the particles, the Froude number of the fountain exceeds unity (figure 6e-h). As a result, once the particles have fallen out, the fluid remaining in the fountain continues to rise (see figure 7h), and the mechanism by which dense fluid accumulates at the top of the fountain is no longer effective. The small amplitude, high frequency oscillations seen in figures 6g and h may be associated with clustering of the particles, perhaps arising from resuspension of particles by the rising fluid.

Although our experiments are relatively simple compared to the fountains which forms during an explosive volcanic eruption (cf. Woods 2010), it is nonetheless of interest to estimate the range of particle sizes for which U is of order 1 in such an event. With source velocities of order 100-150 m/s, source radii of order 100-300 m and initial density in the range 1-10 kg/m³, we estimate that $M \sim 10^8$ m⁴/s², and $B \sim 10^7$ m⁴/s³, leading to a characteristic volcanic fountain speed of order $u_f \sim 30 - 50$ m/s. Depending on the density of the fountain, this speed matches the fall speed of pumice particles with size of order 5-50 cm (Woods 1988). Although noting the simplicity of the model, which neglects the effects of the heating of air entrained into the fountain which can lead to a reversal in buoyancy of the fountain, this scaling suggests that particles larger than 5-50 cm are likely to fall out of a fountain prior to reaching the top of the fountain. Smaller particles may however continue to rise with the fountain fluid, which in some cases may then become buoyant and form a convecting eruption column. We plan to develop this work further to consider some of the additional processes controlling the dispersal of different sized particles in these volcanic flows.

4. Conclusions

We have studied the dynamics of particle-laden fountains, produced by the injection of a mixture of particles and water into a tank filled with water. In the case $U < 0.1$, the fountain behaves as a single-phase fountain and the flow rises to a mean height at which $Fr \approx 1$. The fountain oscillates about this mean height as discrete volumes of fluid build up and then fall to the ground. The frequency of the oscillations coincide with the frequency of oscillations of a fountain issuing from a source with $Fr = 1$ located at a height h_m above the original source, suggesting that the oscillations are controlled by the upper region of the fountain where $Fr < 1$. In contrast, when $U > 0.4 - 0.5$, we have found that for source Froude numbers in the range $6 < Fr_0 < 20$ the particles fallout of the fountain below the height at which $Fr = 1$. As the particles separate from the flow, the fluid continues rising; this suppresses the development of oscillations at the maximum height reached by the particles in contrast to the case $U < 0.1$ which is analogous to a single-phase fountain.

Acknowledgements

This work has been funded through the BP Institute, EPSRC and Hughes Hall, Cambridge. We gratefully acknowledge the technical assistance of A. Pluck, and the constructive comments of three anonymous referees.

REFERENCES

- BAINES, W. D., TURNER, J. S. & CAMPBELL, I. H. 1990 Turbulent fountains in an open chamber. *J. Fluid Mech.* **212**, 557–592.
- BLOOMFIELD, L. J. & KERR, R. C. 2000 A theoretical model of a turbulent fountain. *J. Fluid Mech.* **424**, 197–216.
- BURRIDGE, H. C. & HUNT, G. R. 2013 The rhythm of fountains: the length and time scales of rise height fluctuations at low and high froude numbers. *J. Fluid Mech.* **728**, 91–119.
- CAMPBELL, I. H. & TURNER, J. S. 1989 Fountains in magma chambers. *J. Petrol.* **30**, 885–923.
- CARAZZO, G., KAMINSKI, E. & TAIT, S. 2010 The rise and fall of turbulent fountains: a new model for improved quantitative predictions. *J. Fluid Mech.* **657**, 265–284.
- CARAZZO, G., KAMINSKI, E. & TAIT, S. 2015 The timing and intensity of column collapse during explosive volcanic eruptions. *Earth and Planetary Science Letters* **411**, 208–217.
- HUNT, G. R. & BURRIDGE, H. C. 2015 Fountains in industry and nature. *Annu. Rev. Fluid Mech.* **47**, 195–220.
- LIN, Y. J. & LINDEN, P. F. 2005 A model for an under floor air distribution system. *Energy and Buildings* **37**, 399–409.
- LIU, Q. A. & LINDEN, P. F. 2006 The fluid dynamics of an underdoor air distribution system. *J. Fluid Mech.* **554**, 323–341.
- MCDUGALL, T. 1981 Negatively buoyant vertical jets. *Tellus* **33**, 313–320.
- MINGOTTI, N. & WOODS, A. W. 2015 On the transport of heavy particles through an upward displacement-ventilated space. *J. Fluid Mech.* **772**, 478–507.
- MIZUSHINA, T., OGINO, F., TAKEUCHI, H. & IKAWA, H. 1982 An experimental study of vertical turbulent jet with negative buoyancy. *Warme-und Stoffubertragung* **16**, 15–21.
- ROCCO, S. & WOODS, A. W. 2015 Dispersion in two-dimensional turbulent buoyant plumes. *J. Fluid Mech.* **774**, R1, 1–13.
- TURNER, J. S. 1966 Jets and plumes with negative or reversing buoyancy. *J. Fluid Mech.* **26**, 779–792.
- WILLIAMSON, N., SRINARAYANA, N., ARMPFIELD, S. W., MCBAIN, G. D. & LIN, W. 2008 Low-reynolds-number fountain behaviour. *J. Fluid Mech.* **608**, 297–317.
- WOODS, A. W. 1988 The fluid dynamics and thermodynamics of eruption columns. *Bull. Volcanol.* **50**, 169–193.

Woods, A. W. 2010 Turbulent plumes in nature. *Annu. Rev. Fluid Mech.* **42**, 391–412.